Numerical prediction of brake squeal propensity using acoustic power calculation

S. Oberst, J.C.S. Lai

Acoustic & Vibration Unit,
School Engineering and Information Technology,
The University of New South Wales, Australian Defence Force Academy,
Canberra, ACT 2600, Australia

ABSTRACT

Both low- and high-frequency disc brake squeal, first studied some 80 years ago, remain of concern to automotive NVH departments due to customer warranty claims. Despite both intensive and extensive research, disc brake squeal is still not well understood. It is a very complex problem which involves many different disciplines, such as tribology, structural vibration, acoustic radiation and dynamic instabilities. While there has been considerable research in the first two areas (tribology and vibration analysis), the prediction of brake squeal through acoustic radiation calculations using numerical methods has remained largely unexplored. In this paper, the influence of the geometrical designs of brake pad on brake squeal is studied using a simplified brake setup consisting of an annular disc in contact with one brake pad. The various configurations of a brake pad studied here has been influenced by those used in the industrial testing of a full brake system. In this study, unstable vibration modes were first identified by the conventional complex eigenvalue analysis of a finite element model of the simplified brake system. Then, the acoustic power was calculated for a range of frequencies and friction coefficients using the acoustic boundary element method. It is shown that the performance of the various pads, in terms of brake squeal propensity caused by their geometric differences, could be ranked based on contour plots of acoustic power with friction coefficient and frequency as the independent variables. These results indicate that the inclusion of acoustic power calculations, following a complex eigenvalue analysis of unstable vibration modes, provides improved prediction of brake squeal propensity.

INTRODUCTION

Disc brake squeal is a major concern of the automotive industry Noise, Vibration and Harshness (NVH) departments as well as of customers worldwide. Usually, it appears in a frequency range from $1-20kHz$ (Kinkaid et al. 2003) and is different from brake judder, which is found in a frequency range below $1000Hz$ (Jacobsson 2003). Squeal itself can be separated into sub-groups, namely, low- and high-frequency squeal. The former is generally classified as squeal around $5kHz$ and below the frequency of the first rotor in-plane mode.

The most comprehensive of the review papers on disc brake squeal has been provided by Kinkaid et al. (2003) to address the general problem of brake squeal, the development of analytical, numerical and experimental methods and various mechanisms that underpin brake squeal. The work by Akay (2002) discusses, more particularly, the contact problem and friction-induced noise. The contribution made by Ouyang et al. (2005) focusses predominantly numerical methods in analysing brake squeal. Other literature reviews of the recent years have been written by Papinniemi et al. (2002), Oberst & Lai (2008) and Hoffmann & Gaul (2008), in which state-of-the-art and future challenges are discussed. In this paper, the sound radiation of a simplified brake system, in the form of an annular disc in contact with a pad, is studied. Structural analyses of annular discs are well-known. In a first approximation, annular discs are considered as plates Junger & Feit (1986) which are differentiated as being thin or thick. For a brake rotor, the thin plate theory is usually not applicable. A review of thick plate theories has been written by Liew et al. (1995) and a thick plate's particularly non-linear behaviour has been described by Sathyamoorthy (1983). However, these review articles cover only structural analyses. A comprehensive book, which also deals with the *acoustic properties* of plates and, among other structures, annular discs, has been written by Junger & Feit (1986). However, as stated by Lee & Singh (2005), little is yet known concerning their acoustic radiation. For thick discs, coupling effects between in-and out-of-plane rotor motion become important. Multi-mode excitation is for instance present, when the brake pad slides on the brake disc, as stated by Ewins (2000) and has a strong effect on sound radiation (Lee & Singh 1994). The eigenfrequency becomes dependent on rotational speed and which induces the split of modes hence the coupling of modes is more likely to happen (Cote et al. 1998). Interestingly, an annular disc is able to produce the same in-plane and out-of-plane pattern as a real brake rotor, hence is a suitable simplification (Lee & Singh 2002). The hat structure and its ratio to the rotor thickness and diameter becomes important when considering the coupling between in-& out-of-plane rotor modes (Lee & Singh 2002),(Bea & Wickert 2000). No pad nor friction was considered by Lee & Singh Lee & Singh (2002, 2004, 2005). It was found, that when friction was applied, the bifurcation point only gave highest sound pressure level, which afterwards declined (Oberst & Lai 2009*a*). However, frictional sound caused by rubbing plates of different material against each other has already been analysed by means of radiation efficiencies (Stoimenov et al. 2002, 2005). The authors stated that radiation efficiencies can be used to characterise the acoustic properties of a tribo-system. In another paper by Stoimenov et al. (2005), radiation efficiency was investigated by considering parameter variations between different surfaces in contact. With increasing speed, higher load and greater roughness, the generated noise increased. Due to the roughness, the dominant peaks in the sound signal shifted to a higher frequency. Nowadays, in Noise, Vibration and Harshness (NVH) departments of brake system manufacturers, the Complex Eigenvalue Analysis (CEA) method applied to finite element (FE) model of a brake system is generally accepted as a standard tool for analysing brake squeal, whereby unstable vibration behaviour is identified by a positive real part of the complex eigenvalues (ie, negative damping). It is known that this type of analysis over-predicts the number of unstable modes and not all instabilities are revealed Bajer et al. (2004). Since brake squeal is perceived acoustically and not all unstable vibration modes would result in squeal noise, it seems necessary to have a closer look at the acoustic radiation of a brake

system.

This paper is, therefore, focused on bringing together the techniques of structural vibration finite element method (FEM) and acoustic boundary element method (BEM) in analysing brake squeal. Firstly, a simplified brake system in form of a pad-on-disc system is built and a structural vibration analysis is performed using the commercial software tool, ABAQUS $6.7-1$. Then, the results are transferred to the acoustic boundary element tool of LMS/Virtual Lab Acoustics, which uses Sysnoise 5.6 as its solver. A brief comparison between a pin-on-disc system (Oberst & Lai (2009*a*)Oberst & Lai (2009*b*)) and the newly developed pad-on-disc systems is made. Five pad designs were tested motivated by a design of experiment study (Moore et al. 2008, Oberst et al. 2008). Then the acoustic power is calculated by means of modal superposition of the complex modes by synthesising the frequency response for a concentrated force centred on the pad., Alternatively, the Rayleigh integral is taken and, by means of a plane wave approximation, the radiated sound power in the far-field is calculated. The sound power contour plots, plotted over frequencies and friction coefficients, give an overview of the unstable modes in terms of the brake system's acoustic response.

DESCRIPTION OF MODELS

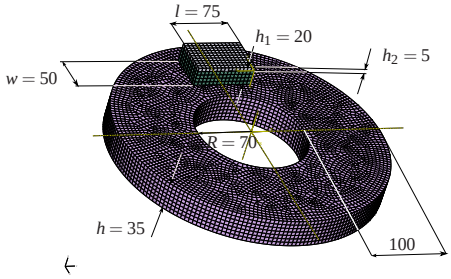

Figure 1: Finite element model of pad-on-disc system

Figure 1 gives the simplified brake system. Some of the reasons for using a simplified brake system are given below.

- *Reduced modal density:* as the modal density is reduced, modal coupling is less often observed so that attention can be focussed on the smaller number of specific coupled unstable modes Cote et al. (1998).
- *Fewer degrees of freedom:* a reduction in brake components results in a reduction of elements, hence, degrees of freedom. This becomes advantageous when calculating the acoustic response by either the BEM or FEM time domain models (Oberst & Lai 2009*a*,*b*).
- *Correlations between methods:* correlations between a time domain and a frequency domain model become feasible in terms of model validation and computational resources required (Oberst & Lai (2009*a*)).
- *Accurate surrogate for brake rotor:* pure in-plane and out-of-plane modes of a real disc can be simulated by means of a generic annular disc (Lee & Singh (2002)).
- Non-symmetric mesh: as the gyroscopic effects are not very strong at low rotational velocities, a non-symmetric mesh allows the effects of mode-splitting to be more pronounced (Ewins (2000)). However, as the modes are not symmetric, a full boundary element (BE) analysis must still be carried out in any case. Hence an unsymmetric mesh is only advantageous.
- Modularity: the system can easily be enlarged by, for instance, changing geometry considering e.g. a hat structure or by installing more brake components which provide for different types of couplings to be studied; for example, introducing the hat leads to in-plane and out-of-plane coupled disc modes (Lee & Singh (2002)).
- Irregular Frequencies: Due to the problem of irregular frequencies which is associated with the BEM (Marburg (2008)), a simplified brake system reduces model complexity and less CHIEF points are required than for real-life structures.

In this paper, five different pad modifications are considered; they are inspired by the pad configurations previously analysed in a design of experiment (DoE) study presented in Moore et al. (2008) and Oberst et al. (2008). Also, the numerical model employed is based on an annular disc in contact with a pad previously used (Oberst & Lai 2009*a*,*b*), which is closer to a pin-on-disc system as the pad is made of steel. In this study, the pad is more realistic, having a lining material and a back plate, and will be referred to as a *pad-on-disc* system. However, the lining material is treated as isotropic, which is not the most appropriate approximation of a real brake pad, and the pressure is still only applied on one side. The five pad configurations are depicted in Figure 2 in which the leading edge is on the right-hand side. The mesh details of the numerical model of

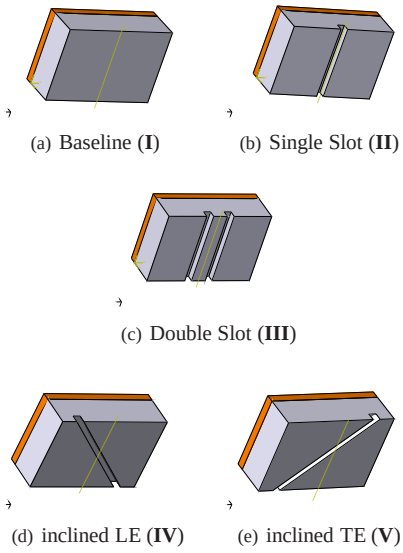

(a) Baseline (**I**) (b) Single Slot (**II**)

(c) Double Slot (**III**)

(d) inclined LE (**IV**) (e) inclined TE (**V**)

Figure 2: Pad designs **I-V**. *LE* & *TE* stand for leading & trailing edge.

Table 1: Mesh details of models (#*EL*:=number of elements)

Model	*EL* (Type)	# *EL* (FEM)	# *EL* Pad	# *EL* (BEM)
I	*C3D8R*	26,163	660	10,088
II	*C3D8R*	26,153	650	10,114
III	*C3D8R*	26,113	610	10,098
IV	*C3D8R*/*D6*	31,355	5760/92	12,272
V	*C3D8R*/*D6*	31,459	5924/32	12,138

Table 2: Material parameters

Parameter	Disc	Lining	Backplate
E *GPa*	110	40	210
ν	0.28	0.10	0.30
ρ kg/m^3	7800	2500	7200

the simplified brake system incorporating five pad configurations are given in Table 1 and 2. Compared to the *pin-on-disc* setup which has 23989 elements for the FE model, the system's mesh is refined for two reasons: firstly, so that modes up to 7*kHz* could be analysed; and secondly, the CEA requires a finer

mesh for all cases as a result of the incorporation of a lining material. A linear hexahedral reduced integration element was chosen with hoursglass controll and second order accuracy. A mesh-convergence study (presented in Oberst & Lai (2009*a*)) has been performed for the pad design (III) and (IV) since it was assumed from experiements that they performed the worst. The baseline (I), the single-slot (II) and the double-slot (III) configurations have identical meshing parameters for the pad. The pads with diagonal slots (IV and V) have to be meshed with the *bottom-up* algorithm and two different element types have to be used: a *C3D8R* linear hexahedral 8−node element and a *C3D*6 linear wedge 6−node element (Das 2007). Another element option, a hexahedral element with imcompatible modes capability was not taken, since especially for a higher amount of elements, the computer running times were up to 74% for the mesh used. The wedge elements were taken to adapt better to the geometry, their total number remained rather low. The number of elements for the lining material in pad designs (IV and V) had to be increased by more than 5000 to obtain a stable convergent solution. However, for all five cases, the disc and back plate have the same number of elements (hexahedral/wedge), being $24,563/490$ for the disc and $150/0$ for the back plate. Here, the wedge elements are adopted in order to keep the mesh quality relatively high thereby using a minimum number of elements for a non-symmetric mesh. The *BE* mesh consists of only $tria3/quad4$ elements. A *small sliding formulation* was assumed with the kinematic constraint contact algorithm and a constant friction coefficient. As the acoustic model is composed of the matrices based on the mesh around the vibrating bodies, an envelope is wrapped around the FE structural mesh to generate the acoustic mesh. Ten elements per wavelength are used throughout the acoustic study. The material properties (Young's modulus, E, Poisson ratio, ν and density, ρ) of the disc, lining and backplate are given in Table 2. The fluid properties, ie, the speed of sound and the fluid's density have been assigned the default values of $c = 340m/s$ and $\rho_f = 1.125kg/m^3$.

STRUCTURAL ANALYSIS

Complex Eigenvalue Analysis

Based on a study of a pin-on-disc system (Oberst & Lai 2009*a*), the pad lining material is changed to be more realistically closer to a pad-on-disc system. However, it has been found that, compared with the pin-on-disc system, numerical stability is much harder to achieve and the system does not converge consistently in terms of unstable frequencies (number and coupled modes). Also, the back plate structure has to be introduced to provide higher stiffness to the back of the lining material which, without it, has been found to distort excessively and the solution would not converge. To perform a stability analysis for a brake system, the common approach is to compute the complex eignenvalues. For this purpose, ABAQUS 6.7-2, which allows for pre-stressed analysis by incorporating non-linear effects in the CEA approach, was chosen. Firstly, the structure was pre-stressed and rotated and then the real eigenfrequencies were extracted. The non-symmetric solver, incorporating non-symmetric friction effects (stiffness matrix), was applied. The real-part of a complex eigenvalue represents damping while its imaginary part represents frequency. If the real part of a complex eigenvalue is positive, then any perturbation will grow with time, indicating instablility. By successively increasing the friction coefficient, bifurcation diagrams could be generated. Instead of presenting bifurcation diagrams (ie, observing how modes' stability change as the friction coefficient changes) as in Oberst & Lai (2009*a*). Figure 3 depicts stable and unstable mode pairs in the form of a root locus plot (ie, real-part (damping) vs imaginary-part (frequency)) for a given friction coefficient for all 5 pad configurations. The disc modes are

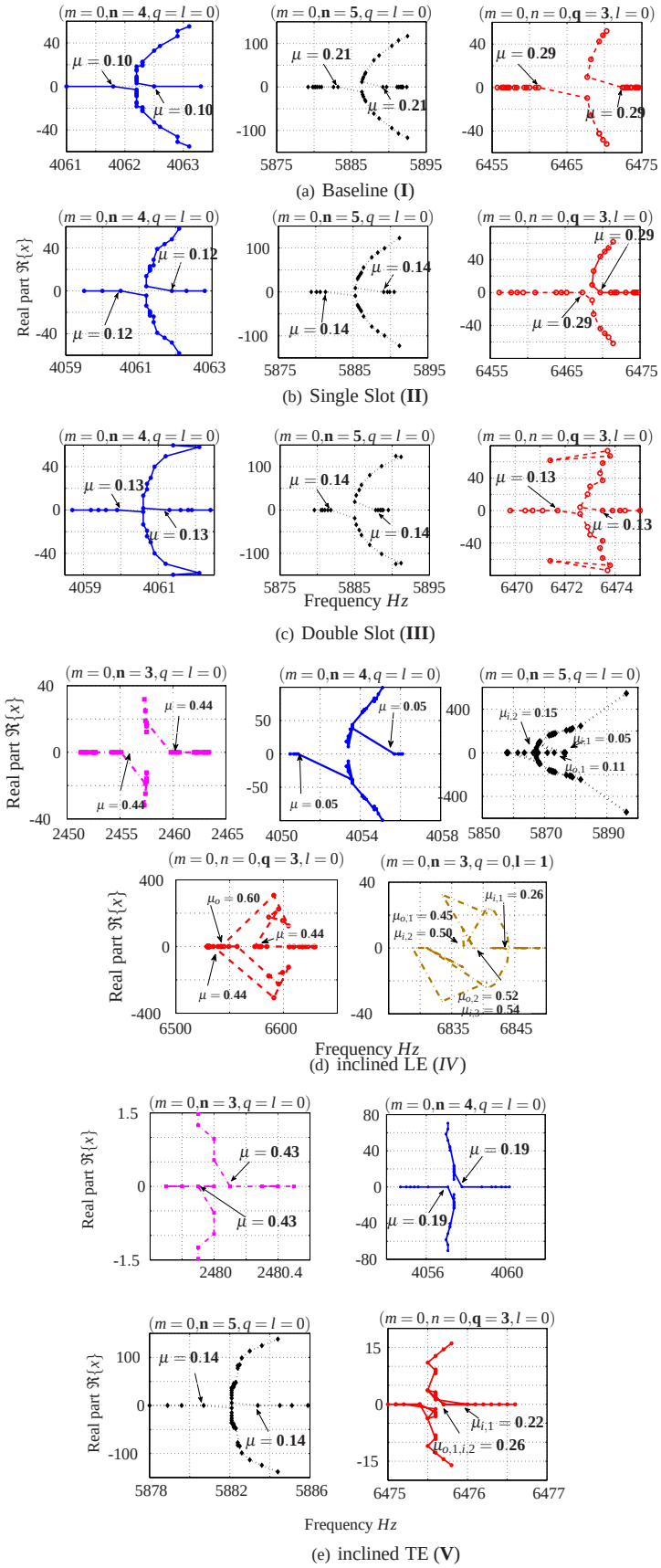

Figure 3: Real part of complex eigenvalues over frequency for pad modifications **I-V**.

characterised by (m,n,q,l), where m, n, q and l are the number of nodal circles and nodal diameters for out-of-plane motion, nodal diameters for radial in-plane motion and nodal diameters for tangential in-plane motion respectively. It is important to distinguish between pure disc modes, coupled pad-disc modes and *unstable* coupled pad-disc modes. A pure disc mode exists only when no other structure is in contact with the brake rotor; otherwise the rotor couples with for instance the pad. If the real-part of the complex eigenvalues of these modes is positive, the coupled disc mode is called *unstable*. Henceforth, only the coupled pad-disc modes are considered here, in accordance with Bea & Wickert (2000). However, for the sake of simplicity, these modes are expressed in terms of the nomenclature used for pure disc modes, since the overall disc's mode shape is often found to be dominant. In all five pad designs, three modes have been identified as unstable: the $(0,4,0,0)$-disc mode; the $(0,5,0,0)$-disc mode, with tangential in-plane pad motion, and the $(0,0,3,0)$-star mode, with very strong tangential in-plane motion of the pad. Furthermore, for the two pads with diagonal slots ($IV-V$), the mode dominated by the $(0,3,0,0)$-disc mode is unstable. A fifth instability occurs at $6.8kHz$ for the pad design IV corresponding to a $(1,2)$-disc mode with an additional in-plane shear component and tangential pad movement. The letters, i and o, used in Figure 3 as subscripts of the friction coefficient μ, stand for *locking **i**n* and *locking **o**ut* respectively. The numbers following refer to the number of locking-in/locking-out events; for instance, $\mu_{i,2}$ indicates a second transition point after having locked out the first time.

Selection of Method for Calculation of Forced Vibration Response

After the CEA, the surface velocities of the structure were generated. The capability of LMS/VIRTUAL LAB, *System Analysis* and three methods implemented in ABAQUS 6.7-1 were tested and the results obtained from the frequency response functions were compared. In general, three criteria are important for the selection of an appropriate method: (i) accuracy, especially *LMS/VL* is not a specialised structural vibration analysis software compared with ABAQUS; (ii) computational expense; and (iii) ease of handling because a considerable amount of calculations has to be performed. A concentrated force of $1000N$ was applied to the middle node of the pad. In Figure 4 three methods implemented in ABAQUS are compared with the subspace method implemented in LMS/VL are compared for the Frequency Response Function (FRF) of the driving point receptance for a pin-on-disc system with three different friction coefficients, $\mu = 0.05$, 0.30 and 0.42. The modal based forced response (**A1**) in ABAQUS calculates the linearised response of the system's steady state due to harmonic excitation and is based on superposition of the system's normal modes. Non-diagonal damping, stiffness and residual modes are not taken into account. The system is pre-stressed due to (i) the pressure applied to the brake disc through the pad and (ii) the disc's rotation at $1.58Hz$. The second method in ABAQUS, the subspace-based steady-state dynamic analysis (**A2**) includes non-symmetric stiffness and damping matrices, hence better suited to calculate the effects of friction. However, no residual modes are included and the system is only represented by a number of complex modes projected onto the subspace . The calculation of FRF implemented in LMS/VL (**L**) works on the same principle. Usually, this method is suitable, if only weak non-linearities are present. Friction effects are strongly non-linear, therefore, this method can only be seen as an approximation and the direct steady-state analysis (**A3**) in ABAQUS should be prefered. This method, based on the calculation of the system response in terms of physical degrees of freedom, is more accurate than both the modal based and subspace method. Although it is the preferred approach to calculate effects of friction and contact, it is computationally expensive. From Figure 4, it can be seen that there are differences in the driving point receptance obtained by the various methods. Even with essentially the same method, ie, subspace method, there are some noticeable differences in the driving point receptance between ABAQUS and LMS implementations. For a given method, the influence of the friction coefficient on the driving point receptance is noticeable. In order to highlight the influence of the friction coefficient for a given method, the normalised differences in the FRF obtained from Figure 4, ie,

$$\Delta FRF_1 = \frac{FRF|_{\mu=0.3} - FRF|_{\mu=0.05}}{FRF|_{\mu=0.3}} \quad (1)$$

$$\Delta FRF_2 = \frac{FRF|_{\mu=0.42} - FRF|_{\mu=0.30}}{FRF|_{\mu=0.42}} \quad (2)$$

which are plotted in Figure 5(a) (a) for comparisons. It can be seen that the influence of the friction coefficient is negligible for the modal based method. While there is some influence of the friction coefficient for the direct ($A3$) and subspace ($A2$) methods implemented in ABAQUS. It is far less significant than the results obtained by the subspace method implemented in LMS. The method provided by *LMS* allows for modal coupling and the major contribution to the differences due to the friction coefficient lies around the frequency $4kHz$. The computing time required to do the forced response calculations with a $2Hz$ frequency resolution for the various methods ($A1$, $A2$, $A3$ and L) using a HP xw4600 workstation with WINDOWS VISTA 64 BIT operating system and $8GB$ of RAM is given in Figure 5 (b). It can be seen that while the direct method (A3) is theoretically the most accurate, the computing time required is almost 4 orders of magnitude of that for the subspace method (L) implemented in LMS. It is clear from Figure 4 that substantial work has to be done in order to ascertain which method is most applicable in the calculating the forced response of a pin-on-disc system. Considering the influence of friction coefficient and the computing resources required, the subspace method in *LMS/VL* has been selected for a preliminary investigation of acoustic power calculations.

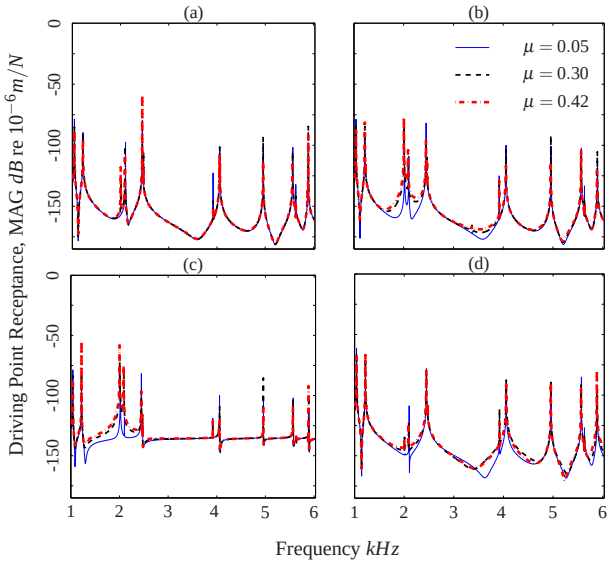

Figure 4: Driving Point Receptances calculated with ABAQUS (a) modal (**A1**), (b) subspace (**A2**), (c) direct (**A3**) and (d) LMS subspace (**L**) for $\mu = 0.05$, 0.30 and 0.42 for the pin-on-disc system (undamped).

ACOUSTIC ANALYSIS

The acoustic analysis was performed using acoustic power calculations based on a plane wave approximation in the far field taking into account of the impedance of the acoustic medium. This is acceptable because in the the model investigated, the bulk of the fluid is moved by the plane surfaces of the disc (Herrin et al. (2003)). Hence, the *Rayleigh* integral could be used to calculate the acoustic power II over an imaginary surface, S in the far-field as follows.

$$\Pi = \int_S I_n dS = \int_S \frac{1}{2} \Re\{p v_n^*\} dS \tag{3}$$

where I_n is the sound intensity, p the sound pressure and v_n^* the transposed complex normal velocity vector. The impedance is that of the acoustic medium, hence, $z_c = \frac{p}{v_n} = \rho c \rightarrow v_n = \frac{p}{\rho c}$.

Comparison pin-on-disc/ pad-on-disc

As an introduction, comparisons of the sound power calculated by both the direct BEM and using plane wave approximation in LMS/VL at $\mu = 0.3$ of the pin-on-disc system as used in Oberst & Lai (2009*b*) with the pad-on-disc simplified brake system are depicted in Figure 6. A viscous damping was applied to the mode set of the brake system to account for internal structural damping effects for two different values: $\zeta = 0.02$ and $\zeta = 0.002$. This damping is frequency dependent and proportional to the velocity. The higher damping value is chosen as an upper bound for some pad modes, which are strongly damped, while the lower damping value accounts for the average value of modal damping values taken from (Papinniemi 2007). It should be noted that in calculating the forced response function using LMS/VL, modal information was imported from ABAQUS and the modal frequencies remain independent of the viscous damping introduced. This was done in order to flatten the forced response functions and to study the effect of this kind of damping. As both the pin-on-disc and the pad-on-disc systems employ discs of exactly the same specifications (Figure 1), the main difference is due to the pad which, despite having the same shape and dimensions, is not a single steel pad as in the pin-on-disc model but is a pad of lining material with a backplate in the pad-on-disc model. It can be seen from Figure 6 that the sound power level for the pad-on-disc system is at least $20dB$ below that of the pin-on-disc system. This is expected because of the strong damping effect provided by the pad's lining material and the backplate in the pad-on-disc system. For a given system, it can also be seen that there is very little difference between the sound power calculated by the Rayleigh integral using the plane wave approximation and the direct exterior BEM and the difference is within 2.5% for the frequency range of interest from $3.8kHz$ to $6kHz$. This result justifies the use of the Rayleigh Integral with the plane wave simplification for the calculation of the acoustic power because the direct BEM would have taken around 10^3 times longer per frequency step to do the calculations for the a BE matrix of ≈ 12500 dof's. In Figure 7, the *acoustic power* as a function of both frequencies and friction coefficient for a slightly damped structure with a viscous damping of 0.2% for the pin-on-disc system is depicted as a $3D$ plot. As shown in Figure 7, it is not easy to examine the details on how the acoustic power changes with frequencies and friction coefficient. It is, therefore, preferable to use contour plots of acoustic power. Contours of the acoustic power over both the friction coefficient and frequencies for the pin-on-disc system and pad-on-disc system (I) with a viscous damping of 2% are compared in (Figure 8). Clearly, a distinguished peak near $4kHz$ is discernible in each case, corresponding to the bifurcation point when two neighbouring modes couple together and get unstable. It is apparent that the pad-on-disc system is subjected to mode-coupling instability at a lower value of the friction co-

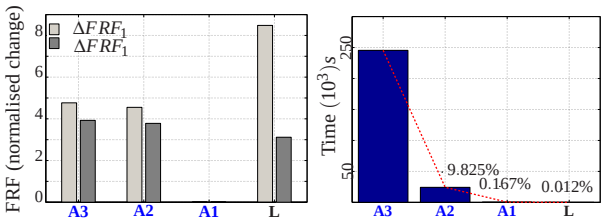

(a) Relative Change (b) Running Time

Figure 5: Performance of several methods compared to calculate surface velocities. **A** stands for ABAQUS and **L** for LMS/VL.

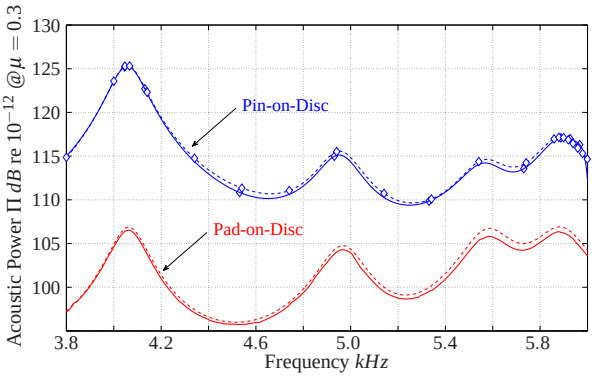

Figure 6: Comparison of simplified **pin-on-disc (-◇-)** and **pad-on-disc (—)** system for $\mu = 0.3$ (Dashed lines $(--)$ give approximations from plane wave approach)

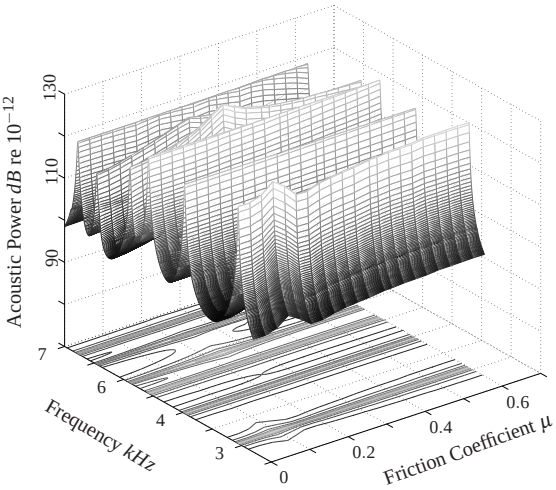

Figure 7: Acoustic power mesh ($\zeta = 0.2\%$) for pad-on-disc (I) system

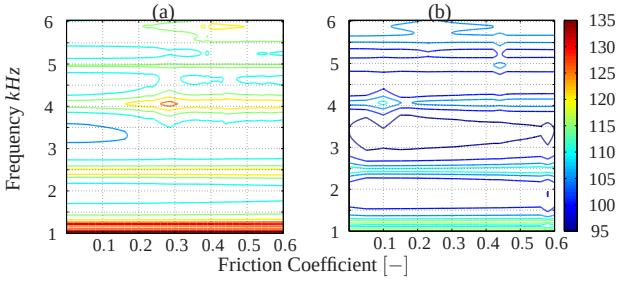

Figure 8: (color online) Contour plots of acoustic power over friction coefficient and frequency for the a) pin-on-disc and b) pad-on-disc (I) for a damping of $\zeta = 2\%$.

efficient (≈ 0.1 vs 0.28) than for the pin-on-disc system. This seems plausible because the softer and more compressible lining material of the pad would attach and couple better to the disc than would a steel pin. Further, the mode at around 2.5 *kHz* for the pad-on-dsic system radiates quite strongly, as can be seen in Figure 8 (b), relative to the unstable mode of $4kHz$, even though this mode at around $2.5kHz$ has not been identified by CEA as unstable. Also, for the pad-on-disc system, there is some change in the pattern of the contours at a friction coefficient of $\mu = 0.58$.

Acoustic Power Calculations for various Pad Designs

In comparing the variation of the acoustic power with frequencies and the friction coefficient for the 5 pad designs in the pad-on-disc system, contour plots for two viscous damping values of 0.2% and 2% are depicted in (Figure 9 and 10) respectively. It should be noted that only the frequency range of $3.8-7.0$ *kHz*, instead of $1-7kHz$, is considered, primarily (i) to reduce the computational time required and (ii) to focus on the unstable vibration modes present in all 5 cases as shown in Figure 3. As a result, the influence of the unstable modes around $2.5kHz$ for the two pad designs (IV and V) is not considered. In Figure 9, the solid vertical lines (magenta) indicate the $\mu-$value for transition to instability. This value is sometimes known the *critical coefficient of friction*, at which the system bifurcates, and the two stable/unstable modes are locked together vibrating with the same frequency. The dashed lines (dark green) indicate the locking-out behaviour of a previously locked-in mode. The contour plots of the pad designs $I-III$, look very similar. One significant difference can be seen in Figure 9 (c) where the ridge at $4050Hz$ maintains its high value over the whole range of μ whereas, in contour plots (a) and (b), the sound power diminishes in the interval between $\mu = 0.1$ and $\mu = 0.2$. However, the acoustic power contour plots in Figure 9(d) and (e) for the the two pad designs with diagonal slots (IV and V) look quite different from those in Figure 9(a)-(c) for designs (I, II and III). It appears that pad design *IV* shows the worst performance with nine peaks. Design *V* has lower overall sound power levels and, also, the number of peaks and ridges with high sound power levels is less than for design *IV* (Figure 9 (d)). It is interesting that, in all cases, the predictions performed using the CEA do not entirely correspond to the acoustic power contour plots, especially at frequencies with high sound power values. For example, in Figure 9(a), three frequencies, at around 4050, 5600 and 5880 *Hz*, show the highest sound power levels whereas, the frequencies predicted by CEA to be unstable occur around 4050, 5880 and 6500 *Hz* (Figure 3(a)) for the baseline pad design (I). At around $6500Hz$ (unstable coupled $(0,0,3,0)$-star mode), the brake system does not appear to radiate very high sound power and at around $5600Hz$, the system emits relatively high energy over the whole range of μ. This strong radiating mode is a $(1,2,0,0)$-disc mode coupled with a pad motion in, predominantly, the in-plane tangential direction due to the negative travelling wave. The split mode of the positive travelling wave, located around $5640Hz$, has a predominantly in-plane radial motion and does not correspond to the ridge with high sound power. In the case of the single slot (II) and double slotted pad (III), the behvaiour is similar to that for pad design (I). The unstable $(1,2,0,0)$-disc mode, which is coupled with a pad moving tangentially to the circumferential circles of the annular disc, dominates the radiated acoustic power(Figure 9(b)-(c)).

From Figure 10, it can be seen that damping the acoustic modes viscously by 2% could be advantageous, as accentuated peaks

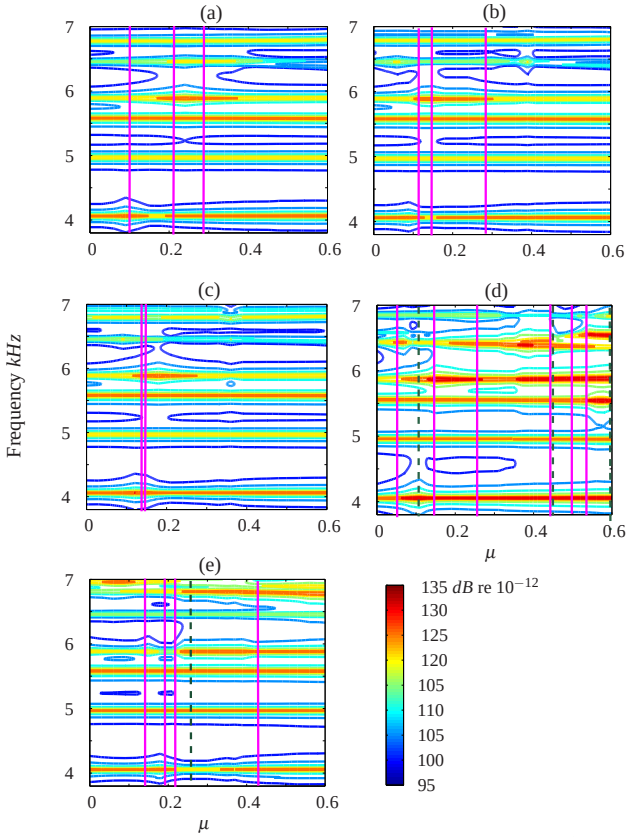

Figure 9: (color online) Contour plots for damping $\zeta = 0.2\%$: (a) baseline model (**I**); (b) single slot (**II**); (c) double slot (**III**); (d) inclined LE (**IV**); and (e) inclinde TE (**V**); vertical lines: solid magenta line '—' represents *locking-in* of two modes and green dashed line '– –' gives value of friction coefficient for a system which locks out

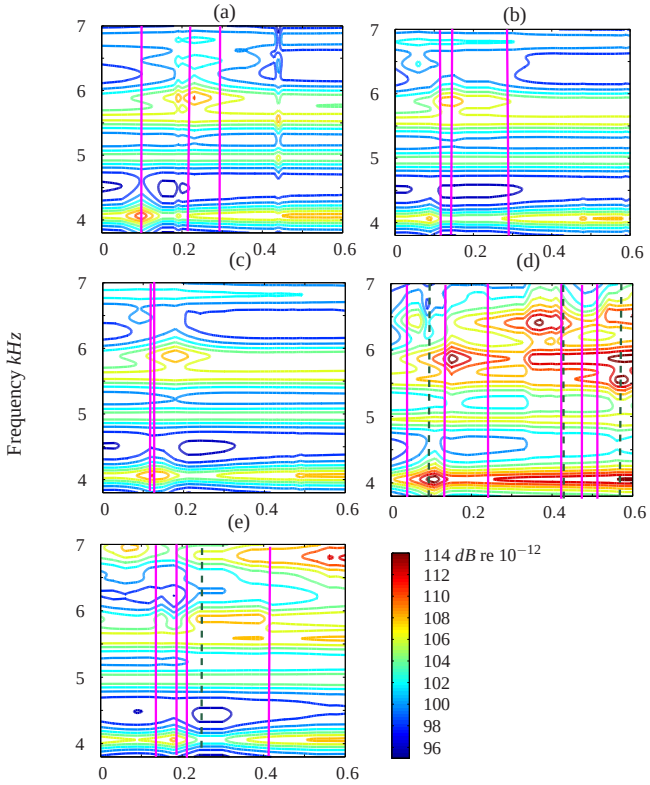

Figure 10: (color online) Contour plots for damping $\zeta = 2.0\%$: a) baseline model (**I**); b) single slot (**II**); c) double slot (**III**); d) inclined LE (**IV**); and e) inclinde TE (**V**); vertical lines: solid magenta line '—' represents *locking-in* of two modes and green dashed line '– –' gives value of friction coefficient for a system which locks out

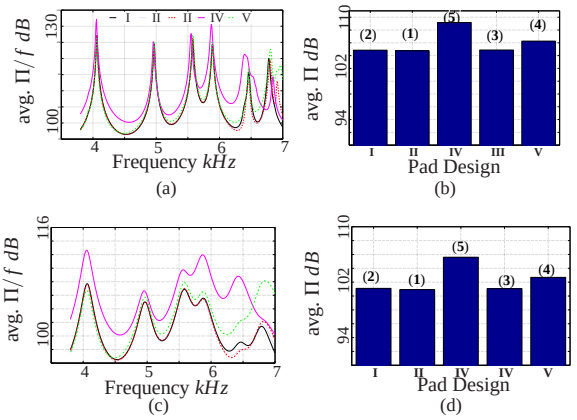

Figure 11: (color online) Acoustic power averaged over friction coefficients for slightly damped case(a) and stronger damped case(c). Average friction coefficient slightly damped (b) and stronger damped modes (d)

are revealed which, previously, are difficult to distinguish from the ridges nearby in Figure 9. The applied damping does not influence the frequency and the system responds rather linearly to this effect *LMS Virtual Lab R8A, help manual* (n.d.). In Figure 10 (a), the baseline model (I) high radiated sound power at three frequencies: around $4kHz$, $5.6kHz$ and $5.8kHz$. However, the mode at $\approx 4kHz$ predicted by the CEA to be unstable, does not show an exposed and dominant ridge in acoustic power. Still, at a friction coefficient of $\mu = 0.44$, a local maximum could be found. The unstable mode at around $4kHz$ has a peak at the bifurcation point of $\mu = 0.1$ which is indicated by the solid vertical line (pink). As μ increases beyond 0.1, the sound power decreases and then peaks again at around $\mu = 0.45$. The sound power of the second predicted unstable mode, at around $5.8kHz$, is maximum only in the region around the predicted bifurcation point at $\mu = 0.21$. However, it is interesting to note that for this unstable mode around 4 kHz, there are two local adjacent peaks and as the friction coefficient increases, the sound power emitted at this frequency attenuates. The pad designs $II + III$ behave very similarly, except that the mode peaking at $5.83kHz$ is not as sharp as for pad design I. Pad design III has a very sharp peak at the bifurcation point ($\mu = 0.12$) of the $(0,4,0,0)$-disc mode with frequency $4061Hz$ compared to pad design II. In terms of the $(1,2,0,0)-$mode, which is quite dominant in the slightly damped case, the graphs in Figure 10a)-c) show a significantly lower sound power level for the more strongly damped case at this frequency. However, a ridge of higher sound power remains in all pad designs (Figure 10(a)-(c). In contrast, pad designs $IV - V$(Figure 2) differ significantly; in particular, pad design IV (slot inclined towards leading edge) shows $6-7$ very high peaks of sound power. The $(0,5,0,0)$ mode at $5880Hz$ seems to be much more dominant than in the pad designs (I-III). Also, at the friction coefficient around $\mu = 0.57$, the $(1,2,0,0)$-disc mode at around $5.6kHz$ has a very sharp peak, although it has not been predicted by CEA to be unstable. It is interesting that the mode $(0,3,0,1)$, predicted to be unstable at around $6.8kHz$, does not show high acoustic power within the range of friction coefficients between 0.01 and 0.6. Astonishingly, this mode becomes visible as it is the global maximum in the acoustic power contour plot for pad design V (Figure 10 (e)) although it is not predicted to be unstable. Intriguing is also that this pad design (V) shows considerable improvement in lower overall radiated sound power over the pad design (IV) of sub-figure 10 (d). The average radiated acoustic power per frequency and overall average (bar diagrams) for five pad designs is shown in Figure 11(d) (a)-(d) for $zeta = 0.2\%$ and 2.0%. In subfigures (a) and (c) the acoustic power was averaged over the 36 friction coefficients, then in (b) and (d) these values were again averaged but over the amount of frequency steps which where 630. The ranks in performance (lower radiated acoustic power the better) are given above the bars. It is obvious that these rankings in terms of average performance are not influenced by the damping. It is possible to extract the best-performing pad which, in both cases, is the one with the single slot (II), and the worst-performing pad, is the one with a diagonal slot inclined towards the leading edge (IV).

Radiation Efficiency of the Pin-on-Disc System

Contour plot of the radiation efficiency of the pin-on-disc system as a function of frequencies and the friction coefficient is shown in Figure 12. It is interesting to see, that the structural vibration modes below the $4kHz$ are very efficient in radiating sound, rather than the unstable vibration modes at $4kHz$ and $5.88kHz$. Also, two local maxima appear, one at a friction coefficient of around $\mu = 0.42$ and $5,3kHz$ and a second from $\mu = 0.5$ to $\mu = 0.6$ at around $4,6kHz$ but they do not correspond to the unstable vibration modes. However, although it is known, that out-of-plane modes with less nodal diameters radiate better (Cote et al. (1998)) the two maxima could pose a problem, especially the one close the the unstable $(0,5,0,0)$-mode at around $5.8kHz$. Anyway, the range below and at $4kHz$ gives over the whole range of friction coefficients high radiation efficiency, hence for a real brake system the problem scope would lie on the unstable $(0,4,0,0)$ mode.

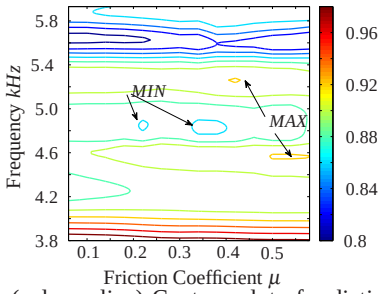

Figure 12: (color online) Contour plot of radiation efficiency of the pin-on-disc system for a damping of $\zeta = 2.0\%$

CONCLUSION

In this study, a previously analysed equivalent pin-on-disc system comprising an annular disc has been extended to a pad-on-disc system by replacing the steel pad with a pad of the same thickness made up of a lining material and a backplate.. The effect of of this pad modification is twofold: (a) in general, the overall acoustic power amplitude is reduced; and (b) the coupling has been enhanced, resulting in a higher number of unstable vibration modes and the bifurcations points shifted to lower μ-values. The effect of 5 different pad designs on brake squeal propensity is studied numerically by identifying unstable vibration modes using complex eigenvalue analysis (CEA) in ABAQUS and calculating the acoustic power of the simplified brake system using LMS/VL subspace method and Rayleigh Integral.. Results of CEA and acoustic power calculations show that not all the peaks in the acoustic power contour plots correspond to unstable vibration modes, similar to the preliminary findings of (Oberst & Lai (2009*a*)) for the pin-on-disc system. It has been shown that by calculating the average sound power for each pad design, the performance of each pad in terms of brake squeal propensity can be ranked with the diagonal slot (IV) being the worst and the single vertical slot (II) being the best. This is coincidentally the finding of an industrial testing of a full brake system with similar pad designs. By considering the complex eigenvalue value analysis, acoustic power calculations and radiation efficiencies together, it ap-

pears that the unstable $(0,4,0,0)$-coupled disc mode is more likely to squeal than the second unstable mode $(0,5,0,0)$ at around $5.8kHz$. These results indicate the potential of predicting brake squeal propensity by including acoustic calculations in addition to traditional complex eigenvalue analysis of unstable vibration modes.

ACKNOWLEDGMENTS

The first author acknowledges receipt of a University of New South Wales University College Postgraduate Research Scholarship for the pursuit of this study.

REFERENCES

Akay, A. (2002), 'Acoustics of friction', *Journal of the Acoustical Society of America* **111**(4), 1525–1548.

Bajer, A., Belsky, V. & Kung, S. (2004), 'The influence of friction-induced damping and nonlinear effects on brake squeal analysis', *SAE Technical Paper* **2004-01-2794**, 1–9.

Bea, J. C. & Wickert, J. A. (2000), 'Free vibration of coupled disc-hat structures', *Journal of Sound and Vibration* **235**(1), 117–132.

Cote, A., Atalla, N. & Guyader, J.-L. (1998), 'Vibroacoustic analysis of an unbaffled rotating disk', *Journal of the Acoustical Society of America* **103**(3), 1483–1492.

Das (2007), *ABAQUS/CAE User's MANUAL*.

Ewins, D. (2000), *Modal Testing: theory, practice and application*, Research Studies Press.

Herrin, D., Martinus, F., Wu, T. & Seybert, A. (2003), 'A new look at the high frequency boundary element and rayleigh integral approximations', *SAE Technical Paper Series* **03NVC-114**, 1–7.

Hoffmann, N. & Gaul, L. (2008), 'Friction induced vibrations of brakes: Research fields and activities', *SAE Technical Paper Series* **2008-01-2579**, 1–8.

Jacobsson, H. (2003), 'Aspects of disc brake judder', *Proc. Instn. Mech. Engrs. Vol. 217, Part D, Journal of Automobile Engineering* **217**, 419–430.

Junger, M. C. & Feit, D. (1986), *Sound, structures, and their interaction (2nd edition)*, Cambridge, MA, MIT Press, 1986, 460 p.

Kinkaid, N., O'Reilly, O. & Papadopoulos, P. (2003), 'Automotive disc brake squeal', *Journal of Sound and Vibration* **267**, 105 – 166.

Lee, H. & Singh, R. (2002), Vibro-acoustics of a brake rotor with focus on squeal noise, *in* 'Internoise 2002, Dearborn, MI, USA'.

Lee, H. & Singh, R. (2004), 'Determiniation of sound radiation from a simplified disc-brake rotor by a semi-analytical method', *Noise Control Engineering Journal* **52**(5), 225–239.

Lee, H. & Singh, R. (2005), 'Acoustic radiation from out-of-plane modes of an annular disk using thin and thick plate theories', *Journal of Sound and Vibration* **282**(1-2), 313–339.

Lee, M. & Singh, R. (1994), 'Analytical formulations for annular disk sound radiation using structural modes', *Journal of Acoustical Society of America* **95**(6), 3311–3323.

Liew, K. M., Xiang, Y. & Kitipornchai, S. (1995), 'Research on thick plate vibration: a literature survey', *Journal of Sound and Vibration* **180**(1), 163–176.

LMS Virtual Lab R8A, help manual (n.d.).

Marburg, Steffen; Nolte, B., ed. (2008), *Computational Acoustics of Noise Propagation in Fluids - Finite and Boundary Element Methods*, Springer Verlag.

Moore, S., Lai, J., Oberst, S., Papinniemi, A., Hamdi, Z. & Stanef, D. (2008), Design of experiments in brake squeal, *in* 'Internoise 2008'.

Oberst, S. & Lai, J. (2008), A critical review on brake squeal and its treatment in practice, *in* 'Internoise 2008, Shanghai'.

Oberst, S. & Lai, J. (2009*a*), Acoustic response of a simplified brake system by means of the boundary element method, *in* 'NOVEM2009, Keble College, Oxford, England, 5-8April'.

Oberst, S. & Lai, J. (2009*b*), Numerical analysis of a simplified brake system, *in* 'NOVEM2009, Keble College, Oxford, England, 5-8April'.

Oberst, S., Lai, J. C. S., Moore, S., Papinniemi, A., Hamdi, S. & Stanef, D. (2008), Statistical analysis of brake squeal noise, *in* 'Internoise 2008, Shanghai'.

Ouyang, H., Nack, W., Yuan, Y. & Chen, F. (2005), 'Numerical analysis of automotive disc brake squeal: a review', *International Journal of Vehicle Noise and Vibration* **1**, 207–231.

Papinniemi, A. (2007), Vibro-acoustic Studies of Brake Squeal Noise, PhD thesis, School of Aerospace, Civil and Mechanical Engineering, The University of New South Wales, Australian Defence Force Academy.

Papinniemi, A., Lai, J., Zhao, J. & Loader, L. (2002), 'Brake squeal: a literature review', *Applied Acoustics* **63**, 391–400.

Sathyamoorthy, M. (1983), 'Nonlinear vibrations of plates. a review', *Shock & Vibration Digest* **3-16**(6), 13pp.

Stoimenov, B. L., Adachi, K. & Kato, K. (2002), Analysis of frictional sound using radiation efficiency, *in* '9th Int. Congress on Sound and Vibration, Orlando, Florida, USA'.

Stoimenov, B. L., Maruyama, S., Adachi, K. & Kato, K. (2005), 'The roughness effect on the frequency of frictional sound', *Tribology*.